ELSEVIER

Journal of Neuroscience Methods 111 (2001) 83–98

JOURNAL OF NEUROSCIENCE METHODS

www.elsevier.com/locate/jneumeth

Comparison of Hilbert transform and wavelet methods for the analysis of neuronal synchrony

Michel Le Van Quyen *, Jack Foucher, Jean-Philippe Lachaux, Eugenio Rodriguez, Antoine Lutz, Jacques Martinerie, Francisco J. Varela [1]

Laboratoire de Neurosciences Cognitives et Imagerie Cérébrale (LENA), Hôpital de La Salpêtrière, CNRS UPR 640, 47 Bd. de l'Hôpital, 75651 Paris Cedex 13, France

Received 29 March 2001; received in revised form 24 April 2001; accepted 25 April 2001

Abstract

The quantification of phase synchrony between neuronal signals is of crucial importance for the study of large-scale interactions in the brain. Two methods have been used to date in neuroscience, based on two distinct approaches which permit a direct estimation of the instantaneous phase of a signal [Phys. Rev. Lett. 81 (1998) 3291; Human Brain Mapping 8 (1999) 194]. The phase is either estimated by using the analytic concept of Hilbert transform or, alternatively, by convolution with a complex wavelet. In both methods the stability of the instantaneous phase over a window of time requires quantification by means of various statistical dependence parameters (standard deviation, Shannon entropy or mutual information). The purpose of this paper is to conduct a direct comparison between these two methods on three signal sets: (1) neural models; (2) intracranial signals from epileptic patients; and (3) scalp EEG recordings. Levels of synchrony that can be considered as reliable are estimated by using the technique of surrogate data. Our results demonstrate that the differences between the methods are minor, and we conclude that they are fundamentally equivalent for the study of neuroelectrical signals. This offers a common language and framework that can be used for future research in the area of synchronization. © 2001 Published by Elsevier Science B.V.

Keywords: Phase synchrony; Neural synchrony; Hilbert transform; Wavelet transform; Surrogate data

1. Introduction

1.1. A brief background on neural synchrony

Synchronization on various levels of organization of brain tissue, from individual pairs of neurons to much larger scales, within one area of the brain or between different parts of the brain, is one of the most active topics in current neuroscience. In particular normal cognitive operations require the transient integration of numerous functional areas widely distributed over the brain and in constant interaction with each other (Damasio, 1990; Varela, 1995; Friston, 1997; Tononi and Edelman, 1998; Varela et al., 2001). Neural synchrony is an important candidate for such large-scale integration, mediated by neuronal groups that oscillate in specific bands and enter into precise phase-locking over a limited period of time. This has, in turn, motivated the search for robust methods for directly measuring such phase-synchrony in this frequency band from experimentally recorded biological signals.

The role of synchronization of neuronal discharges, although not a new idea, has been greatly highlighted by results from microelectrodes in animals (see, e.g. Singer and Gray, 1995; Roelfsema et al., 1997; Neuron, 1999). These single-unit recording studies in animals have been complemented by studies at coarser levels of resolution in humans and animals (Freeman, 1978). These are not spikes, but local field potentials (LFP) of various degrees of spatial resolution, including scalp recording in EEG or MEG. In fact, gamma and beta band responses can be recorded during visual discrimination protocols on the human scalp (Tallon-Baudry et al., 1997) and in subdural electrocorticograms (Le Van

* Corresponding author. Tel.: +331-42-16-1166.
E-mail address: lenalm@ext.jussieu.fr (M. Le Van Quyen).
[1] Deceased.

0165-0270/01/$ - see front matter © 2001 Published by Elsevier Science B.V.
PII: S0165-0270(01)00372-7

Quyen et al., 1997; Lachaux et al., 1999). Also, there is some recent evidence to suggest that not only emission, but also long-range synchronization comparable to those found in single-unit studies in animals can also be detected between surface recordings (Rodriguez et al., 1999). Furthermore, several neurological diseases such as epilepsy (Mormann et al., 2000) and Parkinson's disease (Tass et al., 1998) manifest as a pathological form of the synchronization process.

It is the quantification of phase synchrony between meso- or macro-electrodes (EEG/MEG, intracranial recordings) that requires methods which are entirely different that the cross-correlograms between spike discharges that suffice for microelectrode studies. In this context, it is very important to distinguish very clearly between synchrony as a proper estimate of phase relation, and the classical measures of spectral covariance or coherence that have been extensively used in neuroscience (see, e.g. Bullock and McClune, 1989; Bressler et al., 1993; Menon et al., 1996). As practiced, coherence has two important limitations for our purposes here:

1. First, the classical tools for measuring coherence (Carter, 1987) based on Fourier analysis are highly dependent on the stationarity of the measured signal, which is far from being the case in the brain. The use of time–frequency estimation which does not assume stationarity can go some ways in improving this limitation towards estimating a stable, instantaneous coherence as well as synchrony between two concurrent brain signals.
2. A second and very different limitation is that classical coherence is a measure of spectral covariance, and thus does not separate the effects of amplitude and phase in the interrelations between two signals. Since we are interested in exploring the explicit hypothesis that phase-locking synchrony is the relevant biological mechanism of brain integration, coherence provides only an indirect measure. A direct study of phase relations in the brain requires tools where the phase component can be obtained separately from the amplitude component for a given frequency or frequency range, which can be quite unstable or even chaotic. In brief, coherence provides only a rough indication concerning phase synchrony.

Beyond neuroscience, there has been a general surge of interest in understanding bivariate data by studying their phase synchronization over time (Rosenblum et al., 1999). Thus, although our discussion here is focussed on neuroscience data, its applications can be generalized to other fields.

1.2. Two methods for the study of phase synchrony

Classical synchronization of two oscillators is the adjustment of their rhythmicity, or more precisely, that they manifest phase-locking. More precisely, for signals $s_1(t)$, $s_2(t)$, and their corresponding instantaneous phase $\phi_1(t)$, $\phi_2(t)$, in its most general form the phase locking means

$$n\phi_1(t) - m\phi_2(t) = \text{const} \tag{1}$$

where n, m are integers indicating the ratios of possible frequency locking. In what follows we assume $n = m = 1$ for simplicity, and assume that the constancy of phase difference is valid within a limited window T, typically of a few hundreds of milliseconds.

In the case of neural signals, detecting phase locking between two distant brain recordings (such as EEG, MEG, and intracranial) is not straightforward. This is due to several factors especially when working beyond the single cell level, with neuronal populations from meso- or macroscopic electrodes. Because of volume conduction effects in brain tissues, the activity of a single neuronal population can be picked up by two distant electrodes, which gives rise to spurious phase-locking between their signals. Moreover, in non-invasive signals the true synchronies are buried in a considerable background noise. In this case in the synchronous state the phase fluctuates around some constant value and the question 'synchronous or not synchronous' can only be treated in a statistical sense. This requires new, adapted methods to extract the true synchronies in noisy activities. In this case condition [1] has to be changed to

$$\left|n\phi_1(t) - m\phi_2(t)\right| \approx \text{const} \tag{2}$$

and the degree of approximation estimated as peaks in the distribution of the relative phases in the unit circle over a window T. In brief, for studying phase synchrony two steps are needed: (1) estimate instantaneous phase of each signal; and (2) provide a statistical criteria to quantify the degree of phase-locking.

Both these steps have been independently introduced by two new methods for phase-locking applied to neuronal signals. Tass et al. (1998) treated the original signals by means of a Hilbert transform, and applied to magnetoencephalographic motor signals in Parkinsonian patients (Tass et al., 1998), and to the synchronization between cardiovascular and respiratory rhythms (Schäfer et al., 1998). In contrast Lachaux et al. (1999) treated the original signals by convolution with a complex wavelet, and applied it to EEG and intracranial data during cognitive tasks (Rodriguez et al., 1999; Lachaux et al., 2000a).

Given that a reliable measure of phase-synchrony is an important tool in current research, the purpose of this paper was to conduct a direct comparison between

these two methods on three signals sets: (1) neural models; (2) intracranial signals from epileptic patients; and (3) scalp EEG recordings.

2. Measuring phase synchrony in the brain: a brief review

2.1. Wavelet convolution and (S)PLS

We have recently introduced two complementary methods called phase-locking statistics (PLS) (Lachaux et al., 1999) and single-trial phase-locking statistics (S-PLS) (Lachaux et al., 2000b). Both methods share the same basic procedure: exploiting a complex wavelet to quantify the stability of the phase-difference between two signals in a pre-defined frequency range. However, S-PLS allows us to measure the significance of synchronies in single trials, and does not depend on block repetition of events.

The analysis is always done around a chosen frequency value; the choice is based on a previous detailed time–frequency analysis of the signals which we do not cover here (Lachaux et al., 2000a). Thus a frequency range is defined around this chosen value (e.g. ± 2 Hz), and the subsequent analysis is done on the frequency components of the signals in this frequency range. The procedure is usually iterated in other frequency ranges to cover the whole meaningful part of the spectrum (typically 1–100 Hz).

The first step (common to both methods discussed here) is to measure the instantaneous phase-difference between signals around the frequency of interest. The phase of the signals are extracted from the coefficients of their wavelet transform at the target frequency. These coefficients are the result of a convolution of the original signal with a complex Gabor wavelet (Fig. 1 A). Specifically, let an electrode record a neural signal

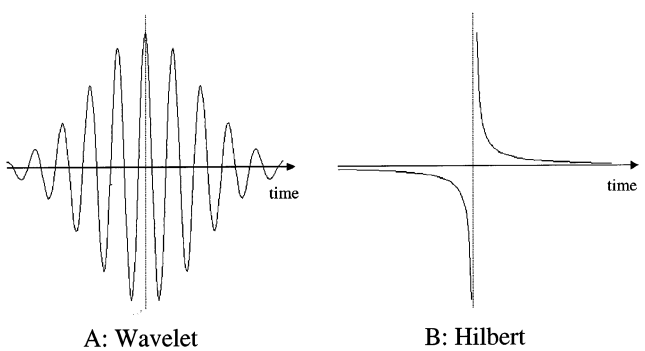

Fig. 1. Two definitions of instantaneous phase. The first way to define the phase of an arbitrary signal is based on the wavelet transform. This can be done via convolution of the signal with a Gabor wavelet (A). Alternatively, the phase can also be obtained via the Hilbert transform defined by convolution of the signal with the function $1/\pi t$ (B).

$x(u)$. Then these wavelet coefficients as a function of time (τ) and frequency (f) are defined as:

$$W_x(\tau, f) = \int_{-\infty}^{+\infty} x(u)\cdot\Psi^*_{\tau,f}(u)\mathrm{d}u \tag{3}$$

Where $\Psi^*_{\tau,f}(u)$ is the complex conjugate of the Morlet wavelet (or Gabor function) defined at frequency f and time τ by:

$$\Psi_{\tau,f}(u) = \sqrt{f}\cdot\exp(i2\pi f(u-\tau))\exp\left(-\frac{(u-\tau)^2}{2\sigma^2}\right) \tag{4}$$

where $\Psi_{\tau,f}(u)$ is the product of a sinusoidal wave at frequency f, with a Gaussian function centered at time τ, with a standard deviation σ proportional to the inverse of f. It depends solely on σ, which sets the number of cycles of the wavelet: $\mathrm{nco} = 6f\sigma$. This value nco determines the frequency resolution of the analysis by setting the width of the frequency interval for which phase are measured. This width is roughly equal to $4f/\mathrm{nco}$ so that the frequency range under study corresponds approximately to:

$$\left[f - \frac{4f}{\mathrm{nco}}, f + \frac{4f}{\mathrm{nco}}\right]$$

For instance at 40 Hz this corresponds to [20,60] Hz, with $\mathrm{nco} = 8$. In most of our studies, we chose nco between 3 and 8.

Now, as a second step, the phase-difference between the signals at frequency f and time τ can be derived from the angles of their wavelet-coefficients.

$$\exp(j(\phi_y(f,\tau) - \phi_x(f,\tau))) = \frac{W_x(\tau, f)W^*_y(\tau, f)}{|W_x(\tau, f)||W_y(\tau, f)|} \tag{5}$$

Both PLS and S-PLS evaluate the variability of this phase-difference across successive measurements. However, PLS is designed to detect stability of phase across the trials, while S-PLS detects stability within each trial. We first developed PLS to estimate phase-locking in experimental situations, common in neurocognitive studies, where a subject is presented with a sequence of similar stimuli. The stability of the phase-differences across the trials, quantified by a phase-locking value (PLV):

$$\mathrm{PLV}(f,t) = \left|\frac{1}{N_{\mathrm{trial}}}\cdot\sum_{\mathrm{trial}=1}^{N_{\mathrm{trial}}}\exp(j(\phi_{y,\mathrm{trial}}(f,\tau) - \phi_{x,\mathrm{trial}}(f,\tau)))\right| \tag{6}$$

where N_{trial} is the total number of trials. PLV is a normalized index, with perfect phase synchrony corresponding to a value of 1. Defined in this way, this index is proportional to the standard deviation of an angular distribution obtained by transforming the relative phase angles onto the unit circle in the complex plane.

As a third and final step, the degree of statistical significance of each phase-locking value is determined by comparing it to values obtained between shifted-tri-

als. These surrogate values are computed from the same signals x and y, using Eq. (5), but after permuting the order of all trials for y, in such a way that the phase differences are no longer computed between signals recorded during the same trial, but during different trials:

$$\mathrm{PLV}_{\mathrm{surrogate}}(f,t) = \frac{1}{K}\sum_{\mathrm{perm}=1}^{K}\left|\frac{1}{N_{\mathrm{trial}}}\cdot\sum_{\mathrm{trial}=1}^{N_{\mathrm{trial}}}\exp(j(\phi_{y,\mathrm{perm(trial)}}(f,\tau) - \phi_{x,\mathrm{trial}}(f,\tau)))\right|$$

We typically create 200 surrogate functions PLV(f,t) from $K=200$ different permutations and measure for each of them their maximum. These 200 values are used to estimate the significance of PLV between original signals x and y. The proportion of surrogate values greater than the original PLV (between x and y) for a time t, is called phase locking statistics (PLS). In most cases, we used a criterion of 5% (PLS < 5%) to characterize significant synchrony.

Recently, we introduced (Lachaux et al., 2000b) a variant of PLS, S-PLS, in order to estimate phase-locking in single-trials, at a slight cost of temporal resolution. In this second method, the variability of phase-difference is not measured across trials, but across successive time-steps, around a target latency. Specifically, a smoothed or single-trial phase locking value (S-PLV) is defined for each individual trial as:

$$\mathrm{SPLV}(f,t) = \left|\frac{1}{\delta}\int_{t-\delta/2}^{t+\delta/2}\exp(j(\phi_y(f,\tau) - \phi_x(f,\tau)))\mathrm{d}\tau\right| \quad (7)$$

As for PLV, S-PLV ranges from 0 to 1 with 1 indicating the strongest phase-locking. The significance of each S-PLV is estimated via a comparison with a distribution of S-PLV obtained between independent Gaussian signals (200 pairs) with the same duration as the original signals generated. For each of them, the maximum S-PLV is measured to build a distribution of 200 values. The proportion of surrogate values higher than the original S-PLV (between x and y) for a time t is correspondingly called single-trial phase locking statistics (S-PLS).

S-PLS depends then on two parameters: nco and the size of the window of temporal integration, which can be expressed in a number of cycles at a chosen frequency f: ncy $= f\delta$. In this sense, ncy determines the temporal resolution of the analysis where the synchrony estimation remains stable. Small values of ncy provide better temporal resolution, and ultimately, S-PLS can match the resolution of PLS with a integration window reduced to one point, but at the cost of statistical resolution because compared to long-lasting episodes, short-lasting episodes of phase-locking are more likely to arise by chance alone. We usually chose ncy between 6 and 10.

2.2. Hilbert convolution and alternative statistics for phase-locking

The instantaneous phase of a signal can also be obtained by means of the analytic signal concept originally introduced by Gabor (1946) and recently investigated for model systems as well as for experimental data (see Rosenblum et al., 1999 for review). For an arbitrary signal s, the analytic signal ζ is a complex function of time defined as:

$$\zeta(t) = s(t) + j\tilde{s}(t) = A(t)e^{j\phi(t)} \quad (8)$$

where the function $\tilde{s}(t)$ is the Hilbert transform of $s(t)$:

$$\tilde{s}(t) = \frac{1}{\pi}\mathrm{P.V.}\cdot\int_{-\infty}^{+\infty}\frac{s(t)}{t-\tau}\mathrm{d}\tau \quad (9)$$

P.V. indicates that the integral is taken in the sense of Cauchy principal value. The instantaneous amplitude $A(t)$ and the instantaneous phase $\phi(t)$ of the signal $s(t)$ are thus uniquely defined by Eq. (8). As can be seen from Eq. (9), the Hilbert transform $\tilde{s}(t)$ of $s(t)$ can be considered as the convolution of the function $s(t)$ with $1/\pi t$ (Fig. 1 B). This means that the Hilbert transform can be realized by an ideal filter whose amplitude response is unity and phase response is a constant $\pi/2$ lag at all frequencies. An important advantage of the analytic approach is that the phase can be easily obtained for an arbitrary broad-band signal. Nevertheless, instantaneous amplitude and phase have a clear physical meaning only if $s(t)$ is a narrow-band signal. Therefore, filtration is required in order to separate the frequency band of interest from the background brain activity.

Following Tass et al. (1998), synchronization of noisy systems is understood as the appearance of horizontal plateaus in the phase difference in time. To characterize statistically the strength of phase synchronization, the deviation of the actual distribution of the phase difference between recording signals from a uniform one must be quantified. For this purpose, a synchronization index based on the Shannon entropy was used:

$$\gamma = (H_{\max} - H)/H_{\max} \quad (10)$$

with the entropy defined by:

$$H = \sum_{k=1}^{N} p_k \ln p_k$$

where N is the number of bins, and $H_{\max} = \ln(N)$ the maximal entropy, and p_k the relative frequency of finding the phase differences within the k-th bin. The optimal number of bins was estimated as $N = \exp[0.626 + 0.4\ln(M-1)]$ where M is the number of samples (Tass et al., 1998). Normalized in this way, we have $0 \le \gamma \le 1$, where $\gamma = 0$ corresponds to a uniform distribution (no synchronization) and $\gamma = 1$ to perfect synchronization.

An alternative phase-locking statistic was introduced in Palus (1997). Let $p_1(\varphi_1)$ and $p_2(\varphi_2)$ be the probability distribution of the phases φ_1 and φ_2, and $p_{1,2}(\varphi_1,\varphi_2)$ their joint distribution. The mutual information

$$I(\phi_1,\phi_2) = \int_{-\pi}^{\pi}\int_{-\pi}^{\pi} p_{1,2}(\phi_1,\phi_2)\log\frac{p_{1,2}(\phi_1,\phi_2)}{p_1(\phi_1)p_2(\phi_2)}\mathrm{d}\phi_1\mathrm{d}\phi_2 \tag{11}$$

is another suitable statistic for testing the dependence between the phases φ_1 and φ_2. The mutual information can be easily rewritten from the entropy $I = H(\phi_1) + H(\phi_2) - H(\phi_1,\phi_2)$. Generally, the mutual information of two processes can be seen as the excess amount of information produced by erroneously assuming that the two systems are independent (Shannon and Weaver, 1949). In the following, we use the normalized mutual information $\rho = I/I_{\max}$ where $I_{\max} = \ln(N)$ and N the number of bins. Normalized in this way, we have $0 \le \rho \le 1$, where $\rho = 0$ corresponds to a uniform distribution and $\rho = 1$ to perfect synchronization. An important feature here is that, in contrast to phase difference statistics, the mutual information provides a general characterization of all possible $n{:}m$ frequency locking.

As a final step, the degree of statistical significance of the phase-locking values was determined in the above studies by comparing them to values obtained from surrogate data. The usual formulation of the null hypothesis is to consider a Gaussian linear process with the same mean, variance and histogram as the series under study. These surrogates are constructed by 'scrambling' the original series. This randomization destroys any temporal structure, if present in the original series. More sophisticated methods imply also preservation of linear correlation between the original data (Palus, 1997), but are not investigated here.

3. Comparative results

This section contains the core of this paper: the comparison between the Hilbert and wavelet approaches using simulated and experimental data. The analysis was performed in the following way: first the signals of overlapping consecutive windows were filtered with a bandpass corresponding to a particular frequency component. Next, the instantaneous phase of each filtered window is extracted by means of wavelet and Hilbert transform. Finally, we characterized the stability of the phase-locking by three measures (as defined before): (1) the standard deviation of the phase differences over the unit circle; (2) the Shannon entropy of the phase differences; and (3) the mutual information of the phases. These indices vary from 0 (no synchronization) to 1 (full synchronization). In order to prevent spurious detection of locking due to noise and bandpass filtering, we derive a significance level by applying our analysis to surrogate data (white noise filtered exactly as the original signals). The 0.95 percentile of the distribution of 200 surrogates, S_{sur}, serves as the significance level. Only the relevant values of the synchrony indices are taken into account by introducing the synchronization index $\mathrm{SI} = \max(S - S_{\mathrm{sur}},0)$, where S is the synchrony measure of the original series. This computation was iterated varying the frequency in 2-Hz steps to cover the whole part of the spectrum from 0.1 to 100 Hz, thus constituting a time–frequency chart of synchrony.

3.1. Phase synchrony in neuronal models

The phase synchronization of two coupled Rössler has been studied (Rosenblum et al., 1996). Unfortunately this chaotic oscillator has a single-peak dominant frequency and thus is not a good model for complex neuronal systems which exhibit a large band of intrinsic rhythms. Instead, we consider here two coupled Hindmarsh–Rose (HR) model neurons (Hindmarsh and Rose, 1984):

$$\dot{x}_1 = y_1 - ax_1^3 + bx_1^2 - z_1 + I - C(x_1 - x_2),$$

$$\dot{y}_1 = c - dx_1^2 - y_1,$$

$$\dot{z}_1 = r[S(x_1 + \chi_1) - z_1].$$

$$\dot{x}_2 = y_2 - ax_2^3 + bx_2^2 - z_2 + I - C(x_2 - x_1),$$

$$\dot{y}_2 = c - dx_2^2 - y_2,$$

$$\dot{z}_2 = r[S(x_2 + \chi_2) - z_2].$$

Each neuron is characterized by three time-dependent variables: the membrane potential x, the recovery variable y, and a slow adaptation current z. The external input is given by I. In the simulation, let $a = 1$, $b = 3$, $c = 1$, $d = 5$, $s = 4$, $r = 0.006$, $\chi_1 = 1.56$, $\chi_2 = 1.57$ and $I = 3$, in accordance to the parameters used in Hindmarsh and Rose (1984). As seen in Fig. 2, the dynamical behavior of this model is characterized by bursts of action potentials on a slow depolarizing wave. Numerical simulation shows that the model is chaotic with maximum Lyapunov exponent of 0.01. Moreover, the HR neuronal model has multiple time-scale dynamics. A fast mechanism (principal frequency approx. 30 Hz in our example) is related to generation of spikes, and a slow mechanism (frequency approx. 3 Hz in our example) related to the bursting process. To examine phase synchronization, we modulated the coupling parameter C. Due to the slight differences in the parameters of the two neurons, their trajectories cannot be identical no matter what the coupling is.

Fig. 2 A shows the simulation results for three typical values of the coupling (state I: $C = 0$, state II: $C = 0.09$, state III: $C = 0.3$). The lower panel (Fig. 2 B) shows the chart of synchronization characterized by the Shannon

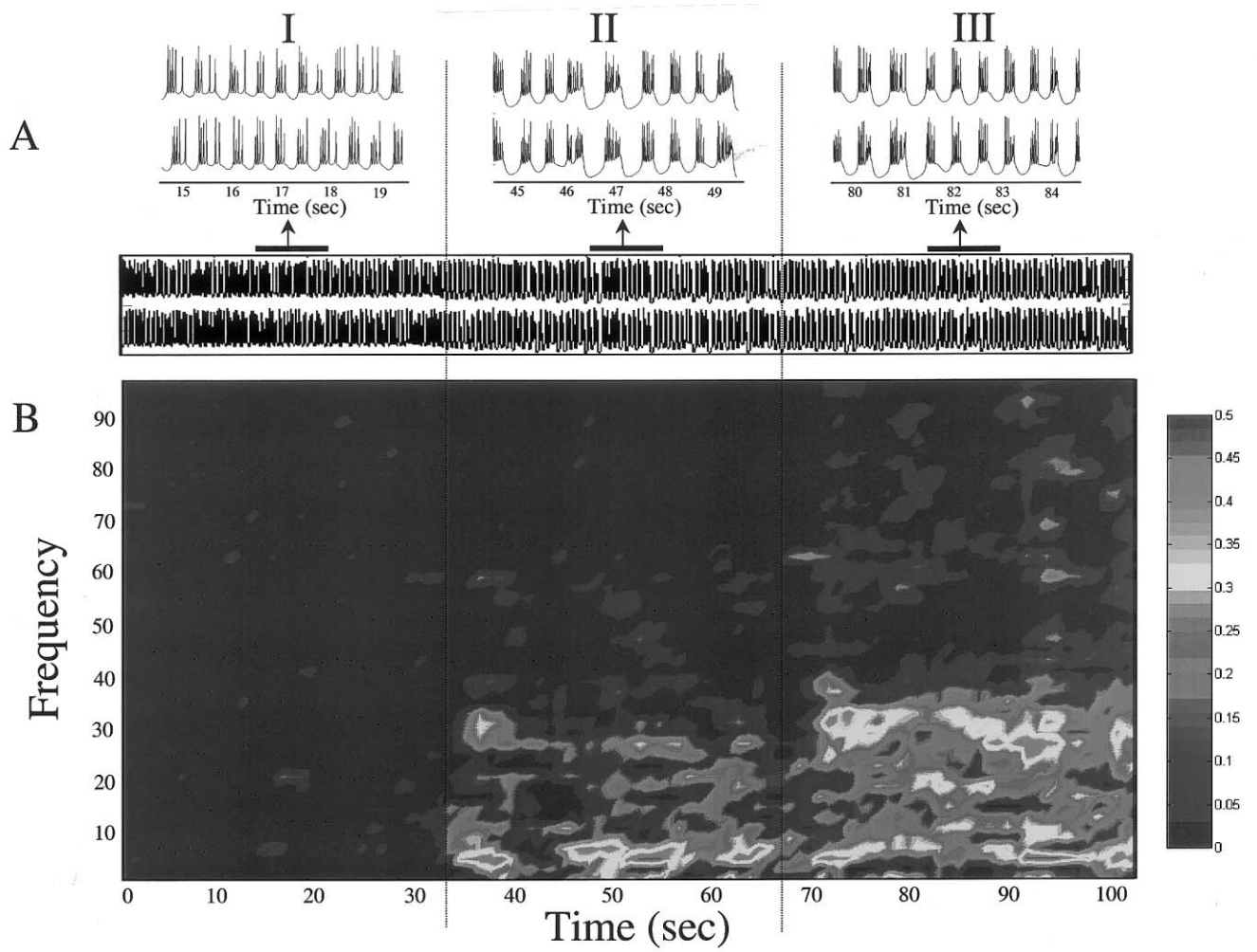

Fig. 2. Phase synchrony between two chaotic neurons. (A) Time course of the two membrane potentials according to the model equations of Hindmarsh and Rose (1984) during three typical values of the coupling (state I: $C = 0$, state II: $C = 0.09$, state III: $C = 0.3$). (B) The corresponding time–frequency charts of synchrony. A sliding window analysis was done with a window length of 1000 points. The distribution of the phase difference was extracted here by wavelet convolution and characterized by the Shannon entropy.

entropy of the phases extracted by wavelets. Without coupling (state I), there is no phase relationship between the neurons (Fig. 2 B). As the coupling strength increase to state II, a transition to synchronous state first appears in the low frequency range (3 Hz) indicating the phase-locking of the slow bursting process. State III again shows synchronies in the low frequency range, but also the occurrence of synchronies in the high frequency range (30 Hz) indicating the phase-locking of the fast spiking process. Because the mean frequency of the two neurons are slightly different, the phase locking shows typical phase slips, i.e. intermittent desynchronization.

In Fig. 3 we compare both approaches using the same simulated data under similar conditions as described before. We see that all different indices reveal the presence of the synchronous states II and III and the application of both extractions of phase leads to practically the same results. Small differences can nevertheless be detected. The synchronies appear sharper at the low frequency range with the phases obtained by means of wavelet transform. Comparing the phase-locking statistics, the mutual information attains higher synchrony values.

We next use a more realistic model to generate network synchronization of gamma and beta rhythms (Fig. 4). This model was first introduced by Ermentrout and Kopell (1998) where it was shown how gamma rhythms support robust synchronization between sites for delays up to 8–10 ms. This long range synchrony requires, as a necessary condition, the occurrence of spike doublets in interneurons. With this model, Kopell et al. (2000) demonstrated that the transition from gamma to beta can be theoretically understood as a consequence of the changes in recurrent excitatory synapses and expressions of K-conductances. For our comparison purpose, we use this minimal network composed by two pyramidal cells (excitatory, or E-cells)

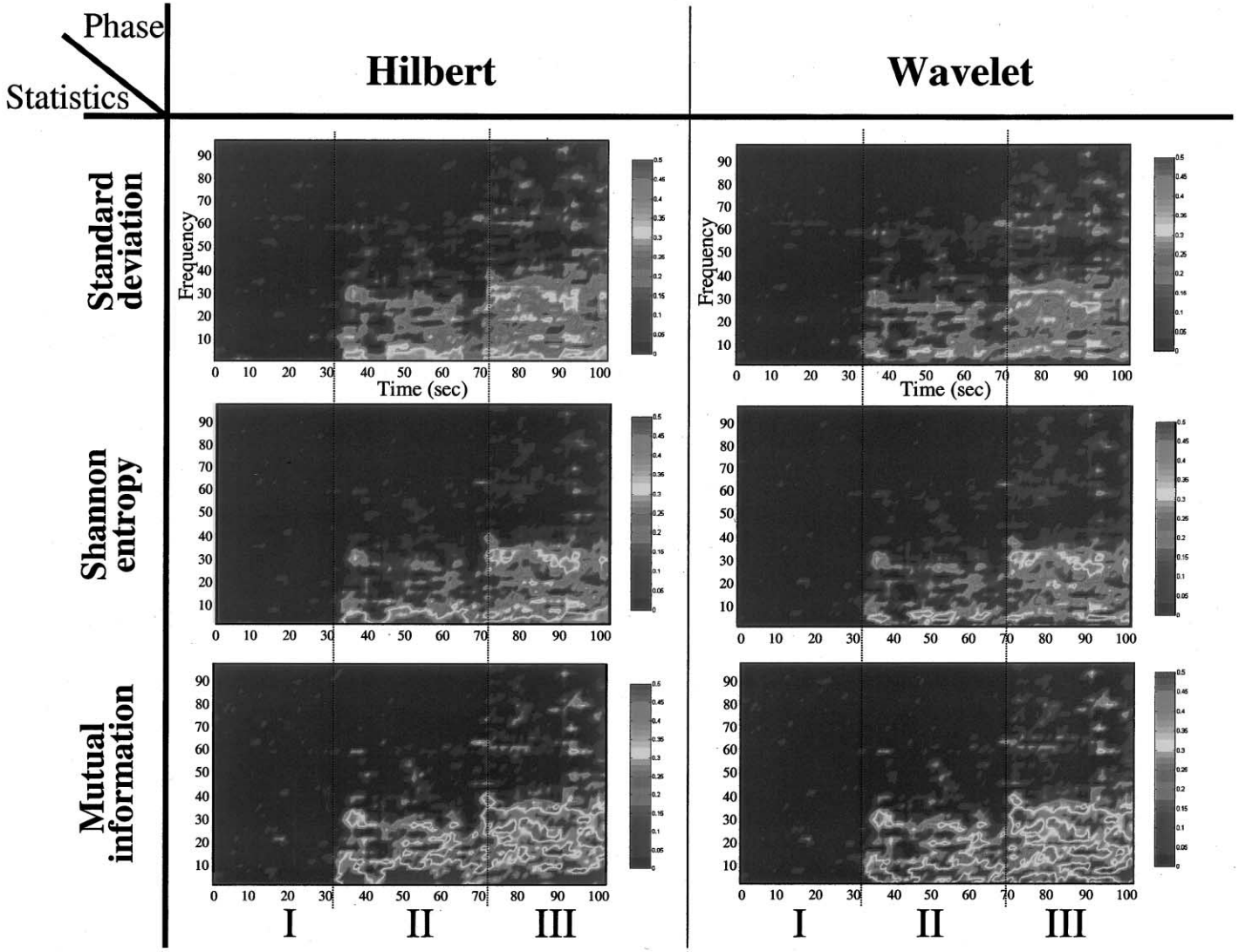

Fig. 3. Comparative results between the two phase extraction techniques (wavelet convolution and Hilbert transform) and three statistics of phase-locking for simulated data (see Fig. 2).

and two interneurons (inhibitory, or I-cells) (Fig. 4 A). Each cell is reduced to a minimal number of currents and modeled as single compartment cells with fast spiking currents for the gamma rhythm; for the beta rhythm, an extra after-hyperpolarization (AHP) current (slow K conductance) is added to the E-cells (see legend of Fig. 4). Increases in K-conductances, plus increases in the strength of synapses between excitatory cells, can transform the output of the network of E and I cells from gamma to beta. This mechanism was confirmed by more detailed biophysical models and experiments (Traub et al., 1999).

Fig. 4 B,C shows the charts of synchrony between the two E-cells for three typical values of excitatory synapses and after-hyperpolarization current. During state I, there is no phase relationship between the

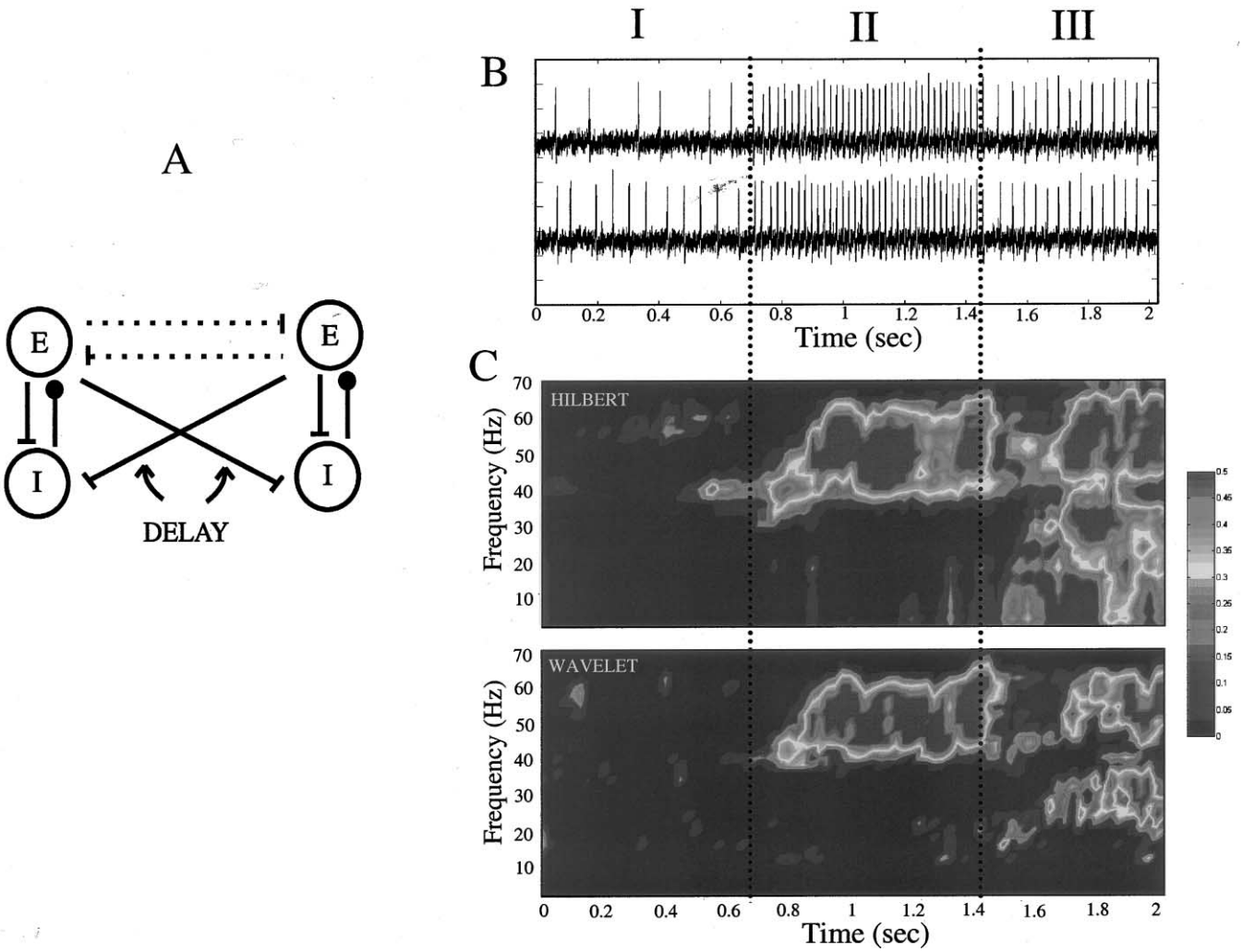

Fig. 4. Phase synchrony in a simulated neuronal network. (A) Minimal network for investigating synchronization with conduction delays. Each excitatory neuron receives input from the local inhibitory neuron and all of the other excitatory neurons; each inhibitory neuron receives input from all of the excitatory neurons and also has self-inhibition. The excitatory neurons satisfy equations of the form: $CV' = -0.1(V+67) - 100m^3h(V-50) - 80n^4(V+100) - g_{AHP}w(V+100) - I^e_{syn} + I^e_{appl} + \eta$ where η is a white Gaussian noise and the variables m, h, n and w satisfy: $m' = 0.32(54+V)(1-m)/[1-\exp(-(V+54)/4)] - 0.28(V+27)m/[\exp((V+27)/5)-1]$; $h' = 0.128\ \exp(-(50+V)/18)(1-h) - 4h/[1+\exp(-(V+27)/5)]$; $n' = 0.032(V+52)(1-n)/[1-\exp((V+52)/5)] - 0.5n\ \exp(-(57+V)/40)$; $w' = (w_{inf}\ (V) - w)/\tau_W(V)$ where $w_{inf}\ (V) = 1/[1+\exp(-(V+35)/10)]$ and $\tau_W(V) = 400/[3.3\ \exp((V+35)/20) + \exp(-(V+35)/20)]$; the inhibitory neurons have identical equations, but there is no AHP current. The capacitance is 1. Synaptic currents are $I^e_{syn} = g_{ie}S_i(t)(V+80) + c_{ee}S_e(t-\delta)$ and $I^i_{syn} = [g_{ei}\ (S^1_e(t) + S^2_e(t)) + c_{ei}(S^1_e(t-\delta) + S^2_e(t-\delta))]V + g_{ii}S_i(t)(V+80)$. In all of the simulations, $g_{ie} = 1$, $g_{ei} = 0.15$, $g_{ii} = 0.2$, $g_{ee} = 0.15$, and $c_{ei} = 0.15$. The synapses satisfy first order equations of the form: $S'_e = 5[1+\tan h(V/4)](1-S_e) - S_e/2$; $S'_i = 2[1+\tan h(V/4)](1-S_i) - S_e/15$. The current applied to the excitatory cells was 6 and 6.5 and acted as the source for the heterogeneity between local networks. The current applied to the inhibitory cells was 1.15. The delay between E-cells is 7 ms c_{ee} (see Kopell et al., 2000 for details). (B) Voltage traces of the two E-cells for three typical values of the coupling and conductance. State I: with $cee = 0$ and $g_{AHP} = 1$, the E-cells miss beats and fires non-synchronously. In this case, the long-range E–E connections are not present to stabilize a synchronous solution with AHP current. State II: with $c_{ee} = 0$ and $g_{AHP} = 0$, the E-cells fire synchronously at a gamma rhythm. State III: $c_{ee} = 0.05$ and $g_{AHP} = 1$, the network quickly suppresses the gamma synchronous solution and transform the output of E from gamma to beta synchronization. (C) Comparative results between the two phase extraction techniques (wavelet convolution and Hilbert transform). A sliding window analysis was done with a window length of 100 ms. The distribution of the phase difference was characterized by the Shannon entropy.

excitatory cells. In state II, we used parameters that elicit gamma synchronies where AHP currents and E–E connections are absent. The synchrony charts obtained by wavelet convolution and by Hilbert transform show clearly the occurrence of synchronies in the gamma frequency range (40–60 Hz). During state III, a slower K-conductance has been added to the model E-cells; now the E-cells, slowed down by the K-conductance, each fire on half of the gamma cycles in the beta frequency range (20–30 Hz). The synchrony charts show the gamma-to-beta transition during this state. The existence of synchronies in the gamma frequency range is due to the phase-locking of subthreshold membrane oscillations.

3.2. Phase synchrony of intracranial recordings during an epileptic seizure

In this section we present an analogous comparison between the two approaches under study for the case of real neuroelectric data: phase synchronization between brain activities during an epileptic seizure. In a first example, Fig. 5 shows the analysis of intracranial EEG recordings taken from a patient presenting a medial temporal lobe epilepsy (Adam et al., 1996). A depth electrode was used to sample the medial structures of the temporal lobe (amygdala and hippocampus) generating the seizure. The post-implantation location of the electrodes was controlled by MRI and the recordings were performed on a 32-channel BMSI system (Nicolet-BMSI, Madison, Wisconsin, USA). The raw data were digitized at 200 Hz and were passed to a 32-channel amplifier system with band-pass filter settings of 0.5–99 Hz. For the study of synchronization, bipolar recording was rejected in favor of monopolar recording with a common reference shown to be quiet (Rappelsberger, 1989). This reference was external and over the ear contralateral to the suspected epileptogenic zone. Here our analysis was limited to the analysis of the channels of the medial temporal lobe that first showed ictal discharges, involving one contact in the amygdala and one contact in the hippocampus body.

Fig. 5 A shows the seizure onset determined by the appearance of low voltage activities at fast frequencies (12–15 Hz) slowed down during the seizure development to 2–3 Hz. The lower panel (Fig. 5 B) shows the chart of synchrony characterized by the Shannon entropy of the phases extracted by Hilbert transform. Before the seizure, the phase relationship between the neuronal activities mostly occur in the gamma range (30–80 Hz). At seizure onset, a transition to synchronous state appears in the 12–15-Hz and low frequency range (3 Hz). During the seizure development, there was a synchronous state at a low frequency range (3 Hz) related with a strong desynchronization in the high frequency range. After the seizure, the chart shows again synchronies in the gamma range (>30 Hz).

Fig. 6 compares the results for both approaches. Again all the indices follow the similar time course of phase-locking and both extractions of the phase leads to practically the same results, although small differences can be detected. Again, the synchronies appear sharper at the low frequency range with the phases obtained by means of wavelet transform. The mutual information again reaches the higher synchrony values.

Fig. 7 presents a complete analysis of multichannel synchronization during the seizure of another patient. The clinical investigation confirmed a seizure focus in the orbitofrontal cortex (Pars orbitalis of F3). A subdural grid was used here to sample the frontal cortex generating the seizure and adjacent functional areas (the subtemporal cortex and central sulcus, see Fig. 7 A). The lower panel (Fig. 7 B) shows the two time–frequency charts of synchrony obtained by each phase extraction and averaged over all possible combinations of electrode pairs (32×32). We see that both approaches give comparable mean synchronies over the grid: At seizure onset, an abrupt transition to a synchronous state appears in the 8–10-Hz range. A few seconds latter, strong synchronies can be observed at multiple high frequencies (25–90 Hz). As the seizure progresses, a trend of progressive decline in the synchronization frequency occurs and finally ends at a low frequency range (3 Hz) before seizure interruption.

Fig. 7 C compares the methods to analyze the spatial distribution of synchronies over the grid, for two frequency ranges (low band: 8–10 Hz, high band: 40–45 Hz) and for six consecutive time windows taken at seizure onset. Very early in the development of the seizure, both approaches show a progressive phase locking in the low frequency range between the epileptic focus (contact 27) and other electrode sites. This confirms that the orbito-frontal region is the primary source of ictal synchronization. A few seconds later, almost all recording sites are driven to a common phase locking. For the high frequency band, the process of locking brain sites appears to start somewhat later, but leads to a similar global synchronous state. Fig. 7 D compares the number of significant synchronies for each time window. We see that the Hilbert transform and the

Fig. 5. Phase synchrony of intracranial recordings during an epileptic seizure. (A) Intracranial EEG recordings of seizure discharges recorded from a human epileptogenic amygdala and hippocampal body. (B) The corresponding time–frequency charts of synchrony. A sliding window analysis was done with a window length of 5 s (1000 points). The distribution of the phase difference was derived from the Hilbert transform and characterized by the Shannon entropy.

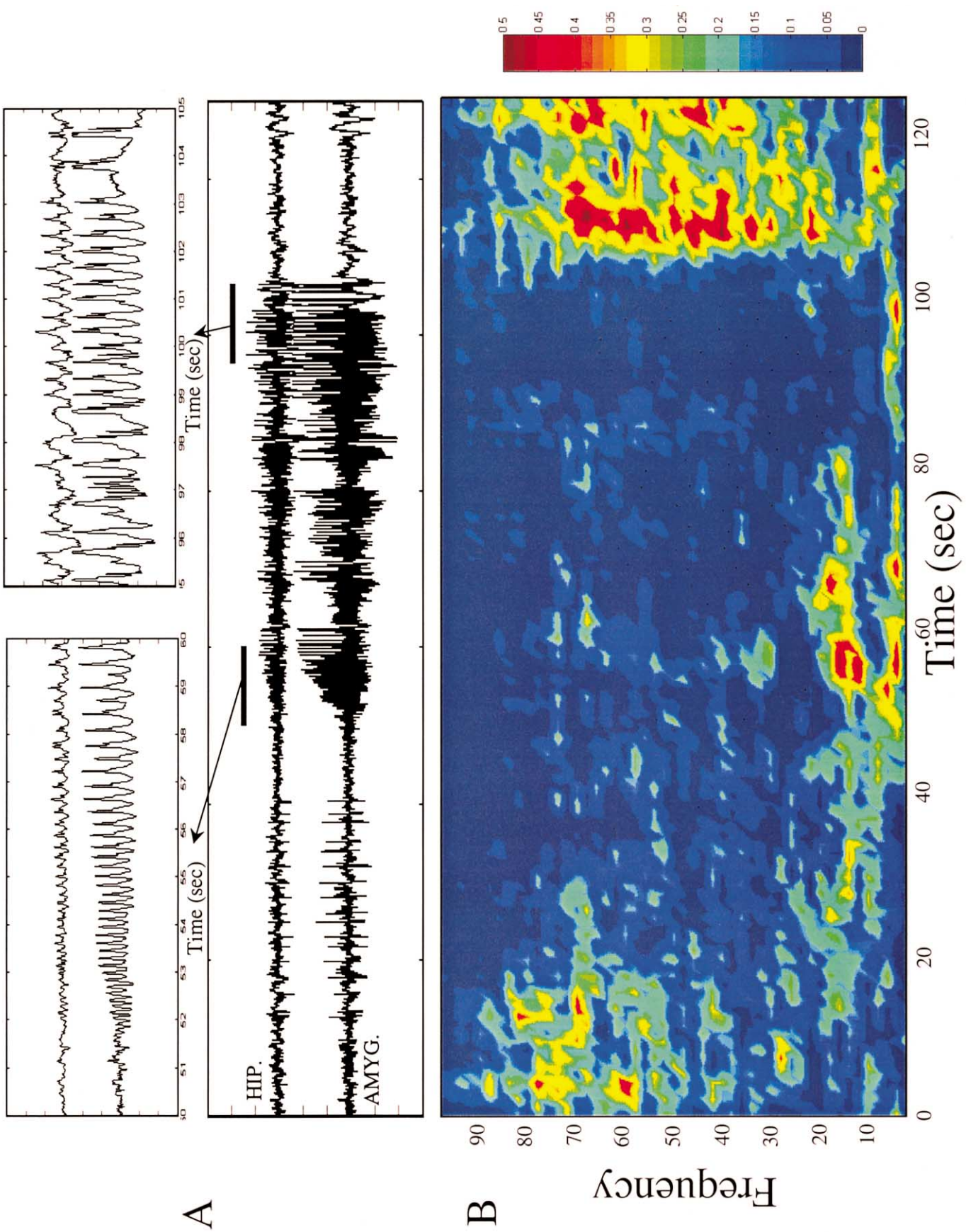

Fig. 5.

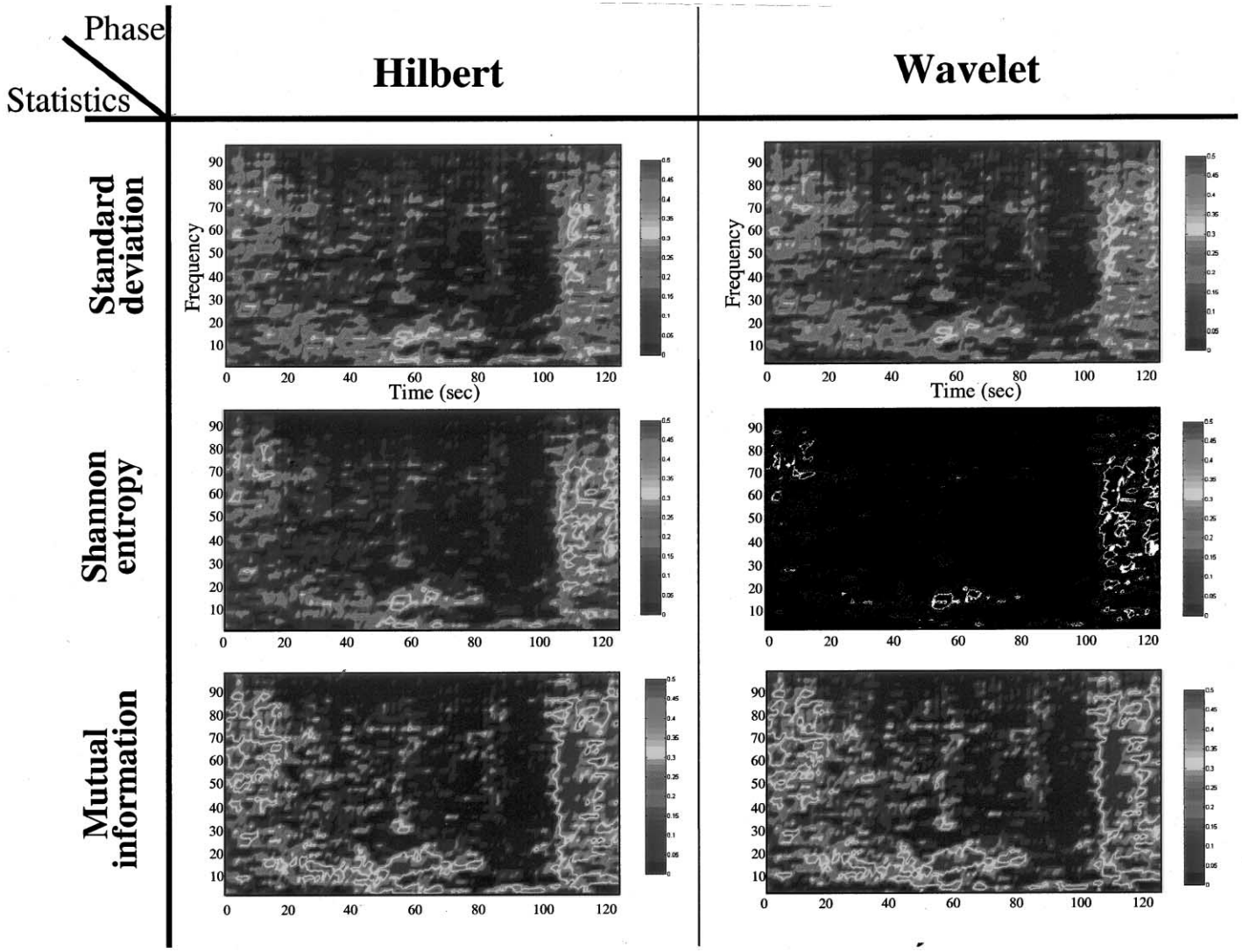

Fig. 6. Comparative results between two phase extraction techniques (wavelet convolution and Hilbert transform) and three statistics of phase-locking for intracranial data (see Fig. 4).

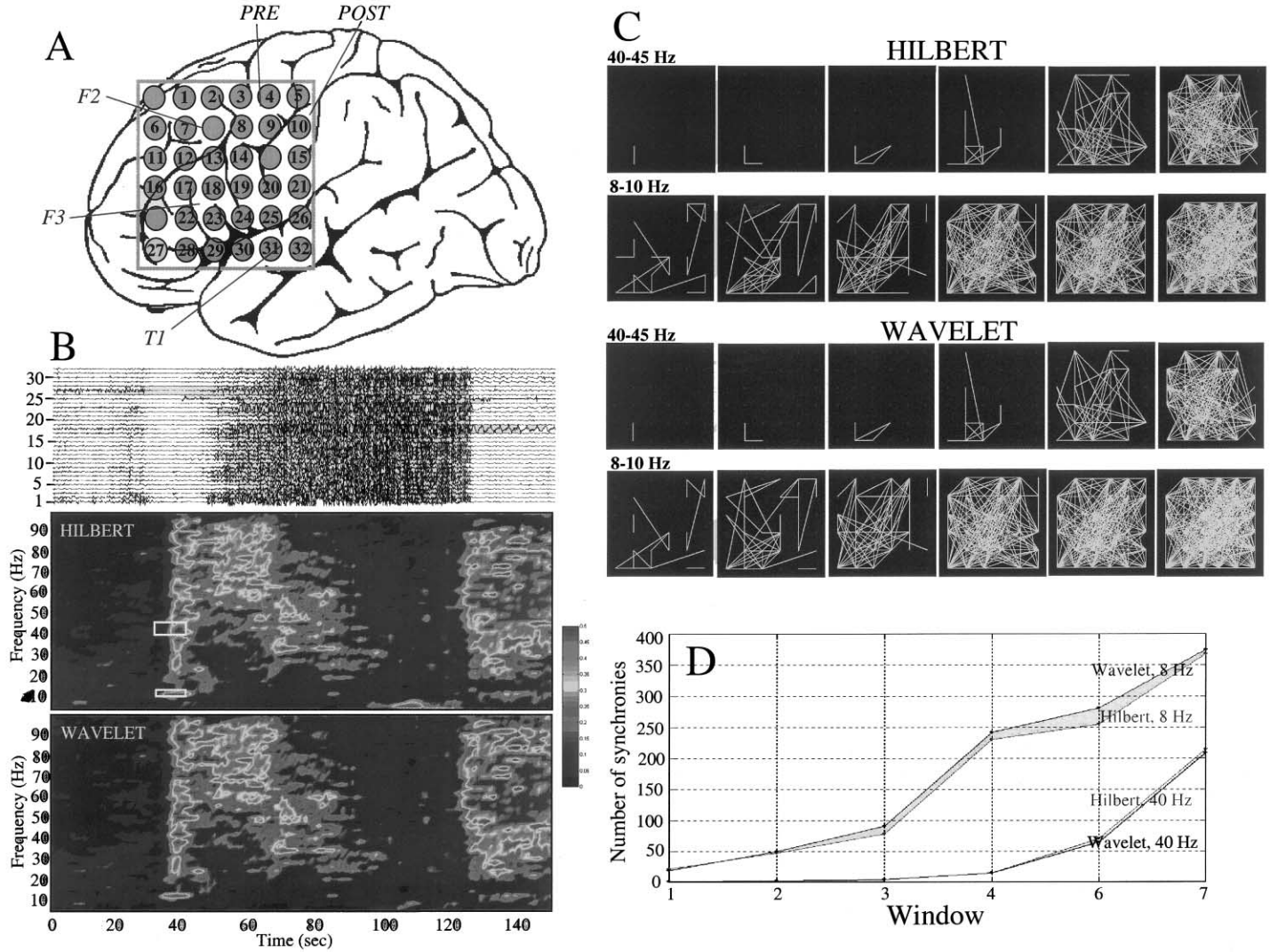

Fig. 7. Phase synchrony of intracranial recordings during an epileptic seizure. (A) A subdural grid with 32 electrodes was used to sample the frontal cortex, adjacent subtemporal cortex and central sulcus (PRE: precentral gyrus, POST: postcentral gyrus) of a patient with an epileptic focus in the pars orbitalis of F3 (contact 27). Inter-electrode center-to-center spacing was typically 10 mm. (B) The two charts of synchrony obtained with wavelet convolution and Hilbert transform and averaged over all possible combinations of electrode pairs. The analysis was done each second with a window length of 5 s (1000 points). (C) Local distribution of synchronies over the grid in the 8–10 Hz and 40–45 Hz frequency ranges for six consecutive time windows at seizure onset (from seconds 35 to 41, see white boxes in B). (D) Number of significant synchronies for the successive time windows.

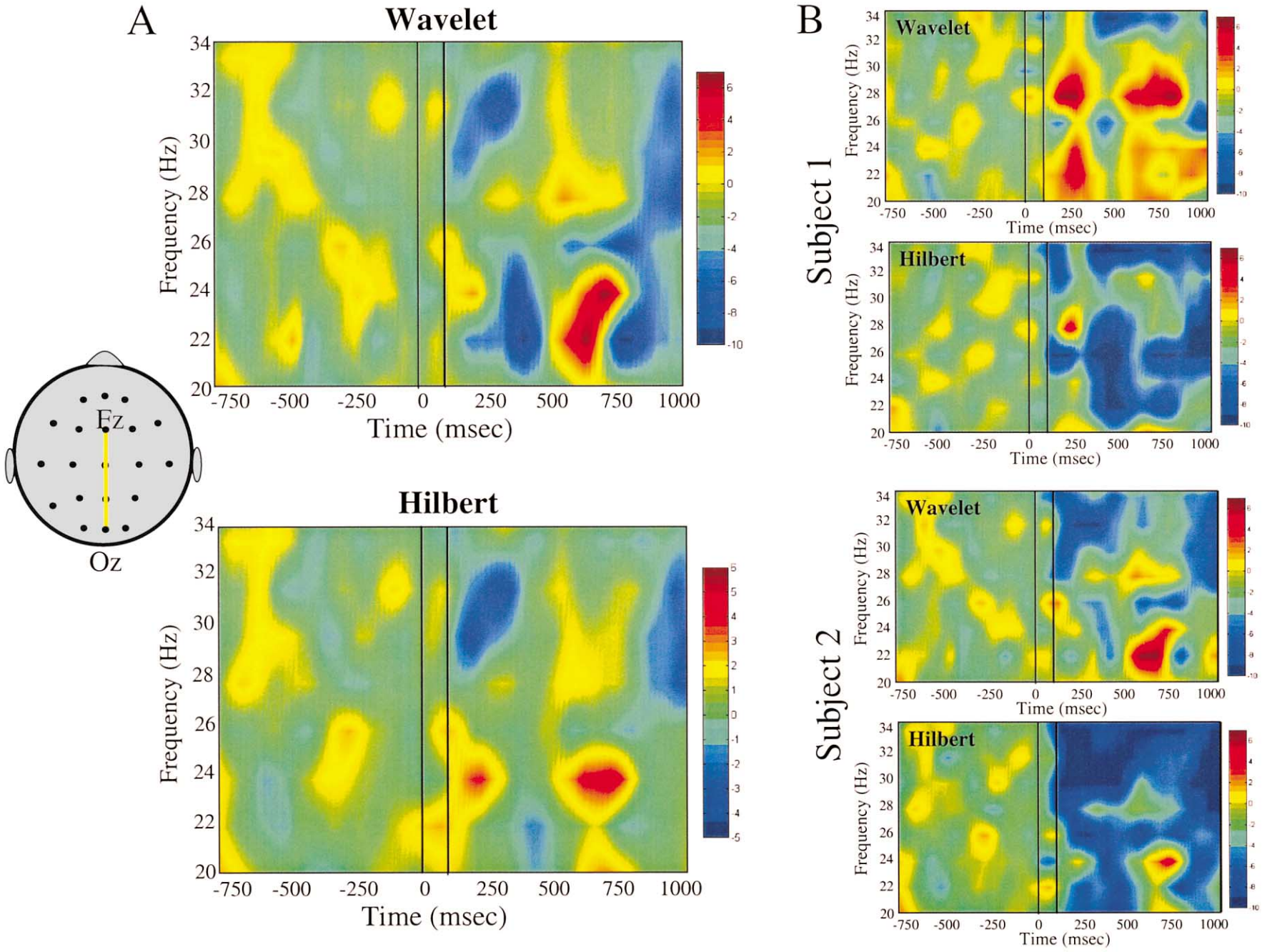
A
Wavelet
Frequency (Hz)
Time (msec)
Ez
Oz
Hilbert
Frequency (Hz)
Time (msec)
B
Subject 1
Wavelet
Frequency (Hz)
Time (msec)
Hilbert
Frequency (Hz)
Time (msec)
Subject 2
Wavelet
Frequency (Hz)
Time (msec)
Hilbert
Frequency (Hz)
Time (msec)

Fig. 8.

wavelet convolutions reveal the same number of synchronies between electrode pairs.

3.3. Phase synchrony of surface EEG recordings during a cognitive task

The last dataset used here for comparison is taken from EEG recordings. Such data are a blurred version of cortical activity and are much more prone to artifacts than intracortical recordings. On the other hand, their non-invasive nature make them an ideal choice for neuro-cognitive studies. Thus it is important to assess which is the best approach for studying phase-locking under these conditions.

In the case of cognitive study, we favor a good time and frequency resolution. Moreover, integrative time windows are adapted to each frequency using the number of cycles as constant. For example, a seven-cycle window as used here will last 233 ms at 30 Hz, but 350 ms at 20 Hz. The resulting number of samples to assess the stability of the phase difference is limited (117 at 30 Hz with a 500-Hz sampling frequency). Here the use of Shannon entropy and the mutual information as synchrony measures have a practical limitation because there should be a minimal number of events falling within each bin to give a reliable estimation. Using the formula proposed by Tass et al. (1998) for Shannon entropy computation, the ideal number of bins using 117 samples is 12. This leads to a rather bad phase angle resolution of 30°, meaning that smaller phase shift during the 233-ms window may be classified in the same bin and thus would not be different from a perfect phase locking. This limitation lead us to only use the standard deviation (PLV) for synchrony estimation.

For our comparison purpose, we studied a representative sample from our study concerning the perception of Mooney faces (see Rodriguez et al., 1999). Mooney figures are made of two-tone asymmetrically lighted photographs of human faces. Ten subjects were shown upright and upside-down Mooney figures had to decide as rapidly as possible whether they perceived a face or not and respond by pressing a two-choice button. EEG was recorded by 30 electrodes at the scalp surface using a 500-Hz sampling frequency.

Fig. 8 compares the two procedures for computing the phase of the signal after the same ± 2 Hz band filtering process (from 20 to 34 Hz every 2 Hz). We have restricted our analysis here to one pair of electrodes (Oz–Fz) because it has been proven to be more active in the perception condition in our previous study, and because the distance between them weakens the risk of false synchrony by pure diffusion. The results are displayed as standard deviation from a reference distribution computed on the pre-stimulus period. For the global intersubject (Fig. 8 A) as well as for all the subject by subject results (Fig. 8 B), the same pattern of synchrony can be seen. Nevertheless, the contrast was systematically better with the wavelet convolution method. This suggests that the wavelet convolution is computationally more efficient for short records.

4. Conclusion

4.1. A general framework for the study of neuronal synchrony

This study has shown that a satisfactory measure of phase synchrony as phase-locking can be obtained with both methods discussed here. From a pragmatic point of view, their differences are minor, and only manifest for small windows of observation. As their computational cost is also comparable, one can safely conclude that they are fundamentally equivalent for the study of neuroelectrical signals. This equivalence might not hold when studying other kinds of signals.

This equivalence can be understood by comparing the common steps in both cases. First, in both cases we are restricting ourselves to a narrow band. Second, in both cases the signals are then convolved with a function with decaying flanks (Fig. 1):

$$\hat{s}(t) = s(t) \otimes \frac{1}{\pi t} \quad \text{or}$$

$$\hat{s}(t) = s(t) \otimes \exp\left(-\frac{t^2}{2\pi\sigma^2} \right) \exp\{ j\, 2\pi f t \}$$

The instantaneous phase $\phi(t)$ defined by $\hat{s}(t) = A(t)\exp(j\phi(t))$ can then be extracted from this new complex signal, thus detaching it from the amplitude component $A(t)$ as needed. Third, in both cases one then applies some statistical measure of significance for the fluctuations: variance, entropy, mutual information. An accurate estimation of the entropy and the mutual information requires a sufficient angular resolution. If it is the case, any one of the measures can be applied as illustrated for intracranial recordings during epileptic

Fig. 8. Phase synchrony of surface EEG recordings during a cognitive task. The Fz–Oz electrode pair synchrony has been computed across the 10 subjects. The signal was pre-filtered between 20 and 36 Hz every 2 Hz. Then, the phase of each signal was computed using the wavelet convolution and the Hilbert transform method. Synchrony was computed using the vectorial summation (PLV). The synchrony chart have the time in ordinate from −750 ms before the stimulus presentation (reference period) to 1000 ms after the stimulus presentation (the Mooney faces were displayed between the two black bares). The values are given in standard deviation from the reference distribution. For the average result across the individuals (A) as well as for two of them (B), the fluctuation of the synchrony from the reference distribution during the post stimulus period are overlapping, but do not have the same contrast intensity, that seems higher with the wavelet convolution.

seizure or model systems. For short records, numerical problems become a decisive factor and the variance (PLV) proved to be computationally more efficient, as illustrated for EEG recordings during a cognitive task.

To summarize, we present direct evidence that the different techniques for quantitative analysis of phase synchronization from neuronal data give similar results. Therefore, the techniques described in this study offer a common framework that can be used for future research in the area of synchronization at different spatial scales, from the single cell level to the level of EEG recordings.

4.2. Directions for future work

The present results indicate that the general framework outlined above allows an examination of neuronal synchronies. However, these techniques must be refined in two directions:

First, despite the fact that the definition of phase synchrony can be formally extended for an arbitrary broad-band signal, a clear physical meaning is only available for narrow-band signals, and filtration is required in order to separate the frequency band of interest from the background brain activity. Nevertheless, it is well known that intracortical field potentials as well as surface recording exhibit a typical $1/f$ spectral distribution, and it is surely the case that there are important interdependencies between the different bands. Such interdependency is another way of stating that brain interactions are highly non-linear (Schiff et al., 1996). Recently, the concept of phase as well as phase synchronization has been generalized for the study of chaotic systems (Rosenblum et al., 1996). Nevertheless, for systems with large variations of the return times (i.e. chaotic attractors having more than one dominant time scale), we do not have access to an unambiguous characterization of the phase as angle coordinate (Brown and Kocarev, 2000). Therefore, a conceptually clear and applicable extension of the definition of phase synchrony to all types of non-linear systems remains to be done.

Second, phase synchrony characterizes the adjustment of intrinsic time scales whereas the amplitude may remain uncorrelated. It is important to stress that phase-locking synchrony is one specific type of synchronization in a variety of other possible ways to understand synchronization between two systems. In fact, multiple definitions of synchrony can be provided depending on the system under investigation and no unified definitions have been established so far (a good review of recent achievements may be found in Brown and Kocarev, 2000). For instance, based on the alternative notion of dynamical interdependence, Schiff et al. (1996) demonstrated that the states of small in vitro neuronal ensembles can be in a functional relationship, called generalized synchronization. This method was recently extended to intracranial recordings of epileptic patients (Le Van Quyen et al., 1999). An important question here is if these new synchronization concepts might prove useful beyond phase-locking synchrony for the analysis of interactions in brain function.

Acknowledgements

We are grateful to B. Pfeuty for his help in the simulations of paragraph 3-1 and Michel Baulac and Vincent Navarro (Unité d'Epileptologie, Hôpital de la Salpêtrière) for providing the clinical data.

References

Adam C, Clemenceau S, Semah F, Hasboun D, Samson S, Aboujaoude N, et al. Variability of presentation in medial temporal lobe epilepsy: a study of 30 operated cases. Ann Neurol Scand 1996;94:1–11.

Bressler SL, Coppola R, Nakamura R. Episodic multiregional cortical coherence at multiple frequencies during visual task performance. Nature 1993;366:153–6.

Brown R, Kocarev L. A unifying definition of synchronization for dynamical systems. Chaos 2000;10:344–9.

Bullock TH, McClune MC. Lateral coherence of the electrocorticogram: a new measure of brain synchrony. Electroencephalogr Clin Neurophysiol 1989;73:479–98.

Carter GC. Coherence and time delay estimation. Proc IEEE 1987;75:236–55.

Damasio AR. Synchronous activation in multiple cortical regions: a mechanism for recall. Semin Neurosci 1990;2:287–96.

Ermentrout GB, Kopell N. Fine structure of neuronal spiking and synchronization in the presence of conduction delays. Proc Natl Acad Sci USA 1998;95:1018–259.

Freeman WJ. Spatial properties of an EEG event in the olfactory bulb and cortex. Electroencephalogr Clin Neurophysiol 1978;44:586–605.

Friston KJ. Another neural code? Neuroimage 1997;5:213–20.

Gabor D. Theory of communication. J EE Lond 1946;93:429–57.

Hindmarsh JL, Rose RM. A model of neuronal bursting using three coupled first order differential equations. Proc R Soc Lond B 1984;221:87–102.

Kopell N, Ermentrout GB, Whittington MA, Traub RD. Gamma rhythms and beta rhythms have different synchronization properties. Proc Natl Acad Sci USA 2000;97:1867–72.

Lachaux JP, Rodriguez E, Martinerie J, Varela FJ. Measuring phase-synchrony in brain signal. Human Brain Mapping 1999;8:194–208.

Lachaux JP, Rodriguez E, Martinerie J, Adam C, Hasboun D, Varela FJ. Gamma-band activity in human intracortical recordings triggered by cognitive tasks. Eur J Neurosci 2000a;12:2608–22.

Lachaux JP, Rodriguez E, Le Van Quyen M, Lutz A, Martinerie J, Varela FJ. Studying single-trials of phase-synchronous activity in the brain. Int J Bifurc Chaos 2000b (in press).

Le Van Quyen M, Adam C, Lachaux JP, Martinerie J, Baulac M, Renault B, et al. Temporal patterns in human epileptic activity are modulated by perceptual discriminations. Neuroreport 1997;8:1703–10.

Le Van Quyen M, Martinerie J, Adam C, Varela FJ. Nonlinear spatio-temporal interdependencies of interictal intracranial EEG

recordings from patients with temporal lobe epilepsy: Localizing of epileptogenic foci. Physica D 1999;127:250–65.

Menon V, Freeman WJ, Cutillo BA, Desmond JE, Ward MF, Bressler SL, et al. Spatio-temporal correlations in human gamma band electrocorticograms. Electroencephalogr Clin Neurophysiol 1996;98-2:89–102.

Mormann F, Lehnertz K, David P, Elger CE. Mean phase coherence as a measure for phase synchronization and its application to the EEG of epileptic patients. Physica D 2000;144:358–69.

Neuron 1999; 24, Cell Press (special volume devoted to reviews on the binding problem).

Palus M. Detecting phase synchronization in noisy systems. Phys Lett A 1997;255:341–51.

Rappelsberger P. The reference problem and mapping of coherence: a simulation study. Brain Topogr 1989;2:63–72.

Rodriguez E, George N, Lachaux JP, Martinerie J, Varela FJ. Perception's shadow: Long-distance synchronization in the human brain. Nature 1999;397:340–3.

Roelfsema PR, Engel AK, König P, Singer W. Visuomotor integration is associated with zero time-lag synchronization among cortical areas. Nature 1997;385:157–61.

Rosenblum M, Pikovsky A, Kurths J. Phase synchronization of chaotic oscillators. Phys Rev Lett 1996;76:1804–7.

Rosenblum MG, Pikovsky AS, Schäfer C, Tass P, Kurths J. Phase synchronization: From theory to data analysis. In: Gielen S, Moss F, editors. Handbook of Biological Physics, vol. 4. Elsevier Science, Neuro-informatics, 1999.

Schäfer C, Rosenblum MG, Kurths J, Abel HH. Heartbeat synchronized with ventilation. Nature 1998;392:239–40.

Schiff SJ, So P, Chang T, Burke R, Sauer T. Detecting dynamical interdependence and generalized synchrony through mutual prediction in a neuronal ensemble. Phys Rev E 1996;54:6708–24.

Shannon CE, Weaver W. The Mathematical Theory of Information. Urbana, IL: University of Illinois Press, 1949.

Singer W, Gray CM. Visual feature integration and the temporal correlation hypothesis. Annu Rev Neurosci 1995;18:555–86.

Tallon-Baudry C, Bertrand O, Delpuech C, Pernier J. Oscillatory gamma-band (30–70 Hz) activity induced by a visual search task in human. J Neurosci 1997;17:722–34.

Tass P, Rosenblum MG, Weule J, Kurths J, Pikovsky A, Volkmann J, et al. Detection of n:m phase locking from noisy data: application to magnetoencephalography. Phys Rev Lett 1998;81:3291–4.

Tononi G, Edelman GM. Consciousness and complexity. Science 1998;282:1846–51.

Traub RD, Whittington MA, Buhl E, Jefferys JG, Faulkner HJ. On the mechanism of the gamma to beta frequency shift in neuronal oscillations induced in rat hippocampal slices by tetanic stimulation. J Neurosci 1999;19:1088–105.

Varela FJ. Resonant cell assemblies: A new approach to cognitive functions and neuronal synchrony. Biol Res 1995;28:81–95.

Varela FJ, Lachaux JP, Rodriguez E, Martinerie J. The brain web: phase synchroniztion and large-scale integration. Nature Rev Neurosci 2001;2:229–39.